Trace element analysis of accessory and rock-forming minerals by ion microprobe (SHRIMP-RG)

Frank K. Mazdab and Joseph L. Wooden

U.S.G.S.-Stanford Ion Probe Laboratory, Stanford, CA 94305 USA
e-mail: fmazdab@usgs.gov; jwooden@usgs.gov

The SHRIMP-RG at the U.S.G.S.-Stanford Ion Probe Laboratory in Stanford, California.
http://shrimprg.stanford.edu

benefits of the SHRIMP-RG:

- *In-situ* micro-analytical measurements permit detailed studies of individual zones within composite grains and minimizes accidental overlap with inclusions.
- SHRIMP-RG combines the excellent spatial and depth resolution of conventional SIMS with the benefits of extreme mass resolution, while maintaining reproducible, flat-topped peaks and high transmission.
- Extreme mass resolution, coupled with limited energy filtering when necessary, permits unparalleled quantification of elements traditionally difficult to measure due to mass interferences, such as Sc and Nb in zircon, and the REE in a variety of rock-forming minerals.
- Well-characterized, matrix-matched synthetic and natural standards are used.

General instrument and acquistion set-up

- O_2^- primary beam; ~1-5 nA beam current; 15-30 μm spot size
- Yα slits and collector slit closed to achieve $M/\Delta M$ >~11000 at 10% peak height, + flat-topped peaks; assessed at $^{45}Sc^+$ in zircon
- testing limited energy filtering to eliminate 5+ atom molecules

NOTES: Not all isotopes listed are measured in all minerals, and in some cases elements have been tested in specific minerals but may not be routinely analyzed. Offset is from listed guide peak, in *amu*. Where noted, offsets may be mineral-specific. Q2 bits drift up or down with time (typically in long period [several week] cycles), but the relative differences between masses remain generally the same.

isotope	Q2 bits	notes
$^{7}Li^+$	3300	not routinely measured in zircon, monazite, xenotime or apatite
$^{9}Be^+$	3180	
$^{11}B^+$	3080	
$^{19}F^+$	2830	
$^{27}Al^+$ ($^{27}Al^{16}O^+$ in Al-rich minerals)	2600	
$^{30}Si^+$	2565	
$^{31}P^+$	2540	offset -0.00784 from $^{30}Si^{1}H^+$ only in P-poor silicates
$^{32}S^+$	2520	offset -0.01775 from $^{16}O_2^+$; not fully resolvable from $^{40}Ca^{24}Mg^{2+}$(17830); not routinely measured
$^{35}Cl^+$	2480	
$^{39}K^+$	2425	not routinely measured in zircon, monazite or xenotime
$^{23}Na^{16}O^+$	2425	not routinely measured in zircon, monazite or xenotime
$^{40}Ca^+$ ($^{43}Ca^+$ in Ca-rich minerals)	2410	
$^{45}Sc^+$	2380	offset -0.01550 from $^{29}Si^{16}O^+$or -0.02376 from $^{28}Si^{16}O^{1}H^+$
$^{28}Si^{16}O^{1}H^+$	2380	offset +0.00826 from $^{29}Si^{16}O^+$; not routinely measured; added as a monitor of H
$^{48}Ti^+$	2340	not measured in titanite due to high count rate
$^{49}Ti^+$	2335	only measured in titanite and zircon
$^{51}V^+$	2325	
$^{52}Cr^+$ ($^{53}Cr^+$ in chromian diopside)	2320	not routinely measured in zircon
$^{55}Mn^+$ ($^{55}Mn^{16}O^+$ in spessartine)	2310	
$^{56}Fe^+$ ($^{57}Fe^+$ in Fe-rich minerals)	2305	added to monitor possible overlap with ilmenite
$^{59}Co^+$	2292	only routinely measured in the ferro-magnesian silicates
$^{60}Ni^+$	2287	offset -0.03596 from $^{28}Si^{16}O_2^+$; only routinely measured in the ferro-magnesian silicates
$^{63}Cu^+$	2270	only routinely measured in the ferro-magnesian silicates
$^{66}Zn^+$	2255	only routinely measured in the ferro-magnesian silicates
$^{69}Ga^+$	2240	not routinely measured in zircon, monazite, xenotime or apatite
$^{74}Ge^+$	2225	offset -0.02443 from $^{28}Si^{30}Si^{16}O^+$
$^{75}As^+$	2220	only measured in monazite, xenotime and apatite
$^{40}Ca^{40}Ca^+$	2210	offset -0.0126 from $^{48}Ti^{16}O_2^+$ only in titanite; monitors Ca dimer production
$^{81}Br^+$	2208	only measured in apatite
$^{40}Ca^{42}Ca^+$	2205	offset -0.0126 from $^{50}Ti^{16}O_2^+$ only in titanite; monitors Ca dimer production
$^{85}Rb^+$	2200	not resolvable from Fe-Si dimers in low Rb minerals; hence, not routinely measured except in Rb-rich minerals
$^{86}Sr^+$	2195	offset of -0.004 minimizes scattered counts from incompletely-resolved Ca-Ca and Ca-Ti (in titanite) dimers
$^{89}Y^+$ ($^{89}Y^{16}O^+$ in xenotime)	2190	not fully resolvable from several Ca-Ti dimers in titanite
$^{93}Nb^+$	2180	offset of -0.0076 minimizes scattered counts from mostly-resolvable $^{92}Zr^{1}H^+$ in zircon
$^{94}Zr^{1}H^+$ (only measured in zircon)	2175	added to estimate potential $^{92}Zr^{1}H^+$ interference on $^{93}Nb^+$ in zircon
$^{96}Zr^+$ ($^{91}Zr^+$ in nominally Zr-free minerals)	2170	
$^{120}Sn^+$	2145	offset -0.0313 from $^{28}Si_2^{16}O_4^+$; not routinely measured in zircon, monazite, xenotime or apatite
$^{133}Cs^+$	2130	not routinely measured in zircon, monazite or xenotime
$^{137}Ba^+$	2120	not routinely measured in zircon, monazite or xenotime
$^{139}La^+$ ($^{138}La^+$ in monazite only)	2115	offset +0.029 from $^{94}Zr^{29}Si^{16}O^+$ in zircon
$^{140}Ce^+$ ($^{136}Ce^+$ in monazite only)	2112	offset +0.025 from average $^{94}Zr^{30}Si^{16}O^+$ and $^{96}Zr^{28}Si^{16}O^+$ in zircon
$^{141}Pr^+$ ($^{141}Pr^{16}O^+$ in LREE-rich minerals)	2110	offset +0.028 from $^{96}Zr^{29}Si^{16}O^+$ in zircon; not routinely measured due to unresolvable interference from $^{140}Ce^{1}H^+$
$^{146}Nd^+$	2107	offset +0.055 from $^{90}Zr^{28}Si_2^+$ in zircon
$^{147}Sm^+$	2105	offset +0.056 from average $^{91}Zr^{28}Si_2^+$ and $^{90}Zr^{28}Si^{29}Si^+$ in zircon
$^{153}Eu^+$	2100	offset +0.051 from average $^{91}Zr^{30}Si^{16}O_2^+$ and $^{92}Zr^{29}Si^{16}O_2^+$ in zircon
$^{165}Ho^+$	2095	
$^{157}Gd^{16}O^+$ ($^{157}Gd^+$ in LREE-rich minerals)	2088	offset -0.0193 from $^{173}Yb^+$ in zircon and xenotime; offset +0.0214 from $^{141}Pr^{16}O^+$ in LREE-rich minerals
$^{159}Tb^{16}O^+$ ($^{159}Tb^+$ in LREE-rich minerals)	2087	offset -0.0205 from $^{175}Lu^+$ in zircon and xenotime; offset +0.02062 from $^{143}Nd^{16}O^+$ in LREE-rich minerals
$^{163}Dy^{16}O^+$ ($^{163}Dy^+$ in LREE-rich minerals)	2085	offset -0.0222 from $^{179}Hf^+$ in zircon; offset +0.01892 from $^{147}Sm^{16}O^+$ in LREE-rich minerals
$^{166}Er^{16}O^+$	2083	
$^{169}Tm^{16}O^+$	2082	
$^{172}Yb^{16}O^+$	2081	
$^{175}Lu^{16}O^+$	2080	
$^{90}Zr_2^{16}O^+$ (only measured in zircon)	2070	added to compare with trace element data collected during U-Pb age determinations
$^{180}Hf^{16}O^+$	2070	
$^{181}Ta^{16}O^+$	2070	offset -0.02364 from $^{197}Au^+$; not routinely measured in zircon due to unresolvable interference from $^{180}Hf^{16}O^{1}H^+$
$^{205}Tl^+$	2055	not routinely measured
$^{206}Pb^+$ ($^{208}Pb^+$ in minerals with only common Pb)	2050	offset +0.165 from $^{94}Zr^{96}Zr^{16}O^+$ in zircon
$^{232}Th^{16}O^+$	2030	
$^{238}U^{16}O^+$	2025	
96	2175	added to assist stepdown to Be
30	2565	added to assist stepdown to Be
18	2800	added to assist stepdown to Be
11	3080	added to assist stepdown to Be
8	3250	added to assist stepdown to Li

ZIRCON

- Progress in technique development:
  effectively complete
- Critical mass interferences:

Sc:

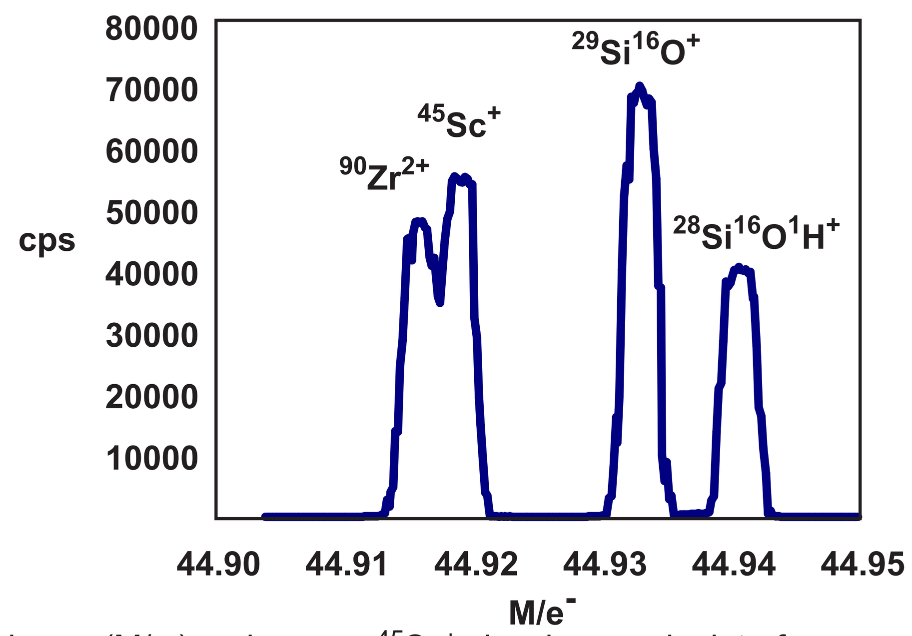

Mass/charge (M/e$^-$) region near $^{45}Sc^+$ showing nearby interferences. M/ΔM = ~11000 at 10% peak height sufficiently resolves $^{45}Sc^+$ from $^{90}Zr^{2+}$ and maintains flat-topped peaks and high transmission.

Nb: $^{92}Zr^1H^+$ especially in metamict zircon

- Standards development:

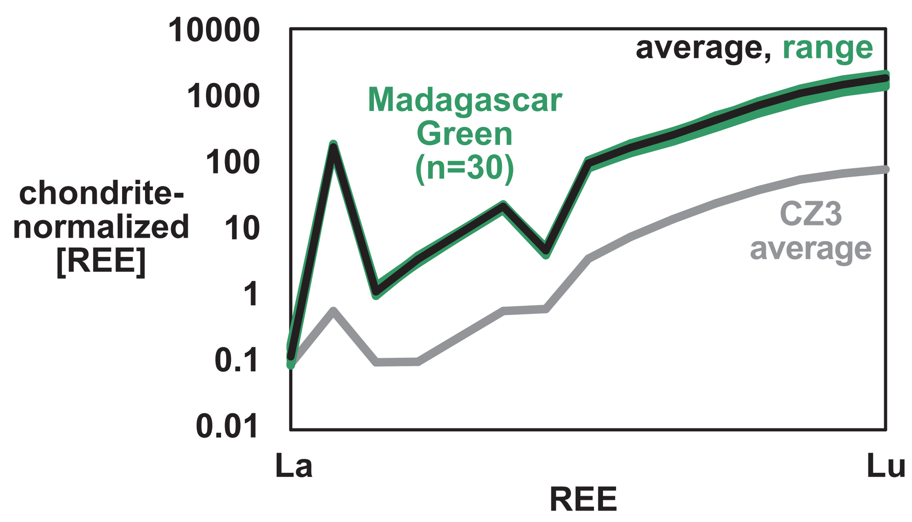

Natural zircon such as the gem grade Madagascar Green is both rich in trace elements and homogeneous (<~10% 1σ). After additional examination, this zircon will replace the Sri Lanka megacryst CZ3 as our primary zircon trace element standard. CZ3 is homogeneous but is unsuitably low in trace elements.

TITANITE and APATITE

- Progress in technique development:
  substantially complete
- Critical mass interferences:

Sc: $^{90}Zr^{2+}$ in high Zr-titanite (see zircon)

Sr & Y: Ca-Ca dimers(titanite & apatite) and Ca-Ti dimers (titanite)

Zr & Nb: Ca-Ca and Ca-Ti dimers in titanite

Tb: $^{48}Ca^{31}P^{16}O_5{}^+$ and $^{40}Ca_2{}^{31}P^{16}O_3{}^+$ in low REE apatite

- Standards development:
  poor but improving
- Example data:

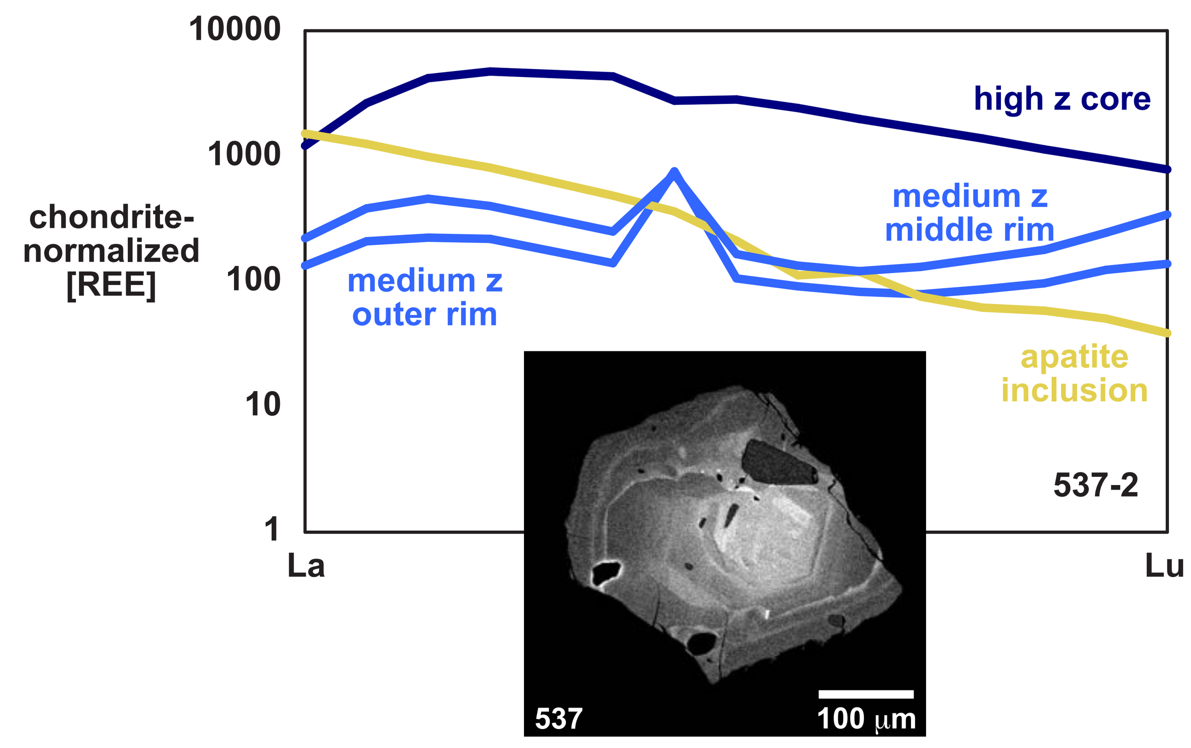

REE plot of apatite and zoned titanite from granodiorite from Joshua Tree National Park, CA, USA (*courtesy of Andy Barth*). Back-scattered electron (BSE) images of compositional zoning in titanite. Higher average atomic number (high z) zones are bright; low z zones are darker gray. Large dark gray inclusion is apatite.

MONAZITE & XENOTIME

- Progress in technique development:
  in progress
- Critical mass interferences:

Sc: $^{90}Zr^{2+}$ in high Zr-xenotime (see zircon)

- Standards development:
  moderate; good for REE but poor for other elements
- Example data:

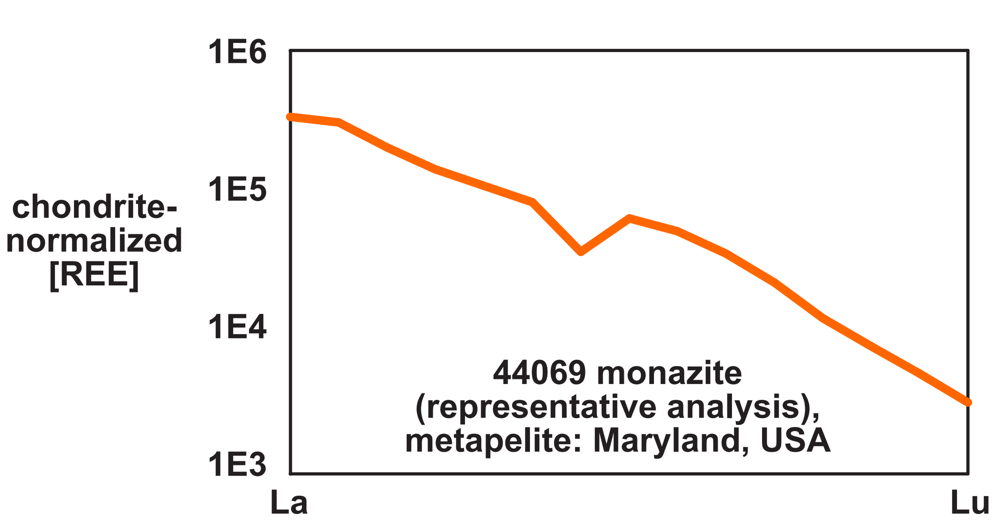

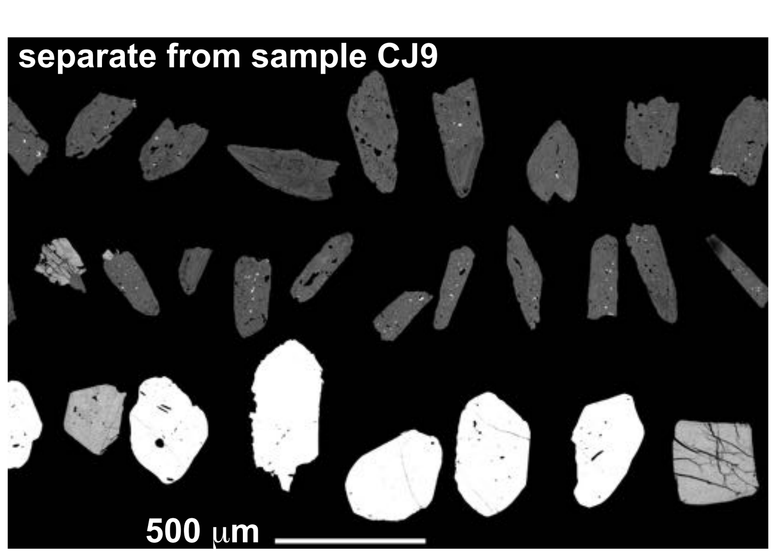

Back-scattered electron (BSE) image of zircon (top two rows, medium gray), monazite (white, bottom row) and xenotime (light gray, bottom row) from Christiansen Ranch pegmatite, Ruby Range, MT, USA (*courtesy of Clayton Loehn and Carson Jones*). Note intergrowth of zircon and xenotime (second row, left). In principle, the distribution of REE among the three minerals can be used to ascertain such intensive parameters as crystallization temperature.

PYROXENE, GARNET, EPIDOTE & OLIVINE

- Progress in technique development:
  in progress
- Critical mass interferences:

Rb: Fe-Si and Mn-Si dimers

Sr, Y, Zr & Nb: Ca-Ca and Ca-Ti dimers

REE: Ca-Fe-(Al)-(Mg)-Si-O polymers

- Standards development:
  poor but improving

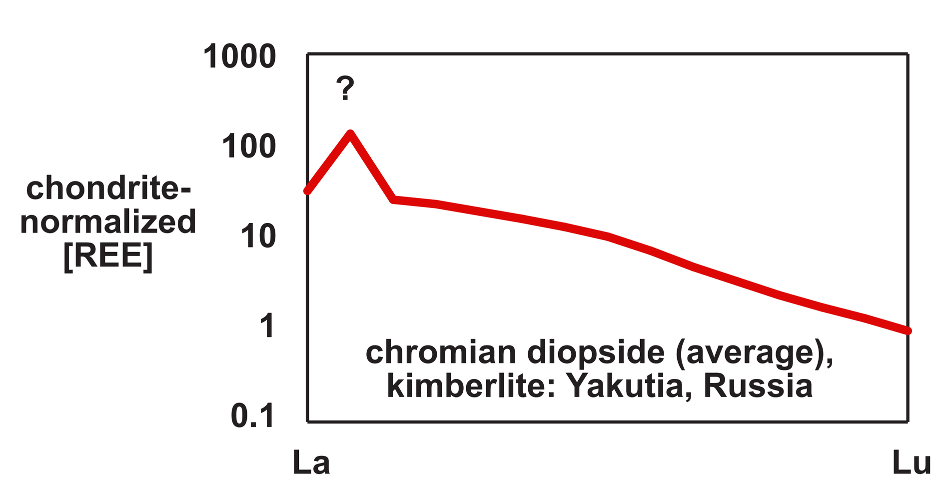

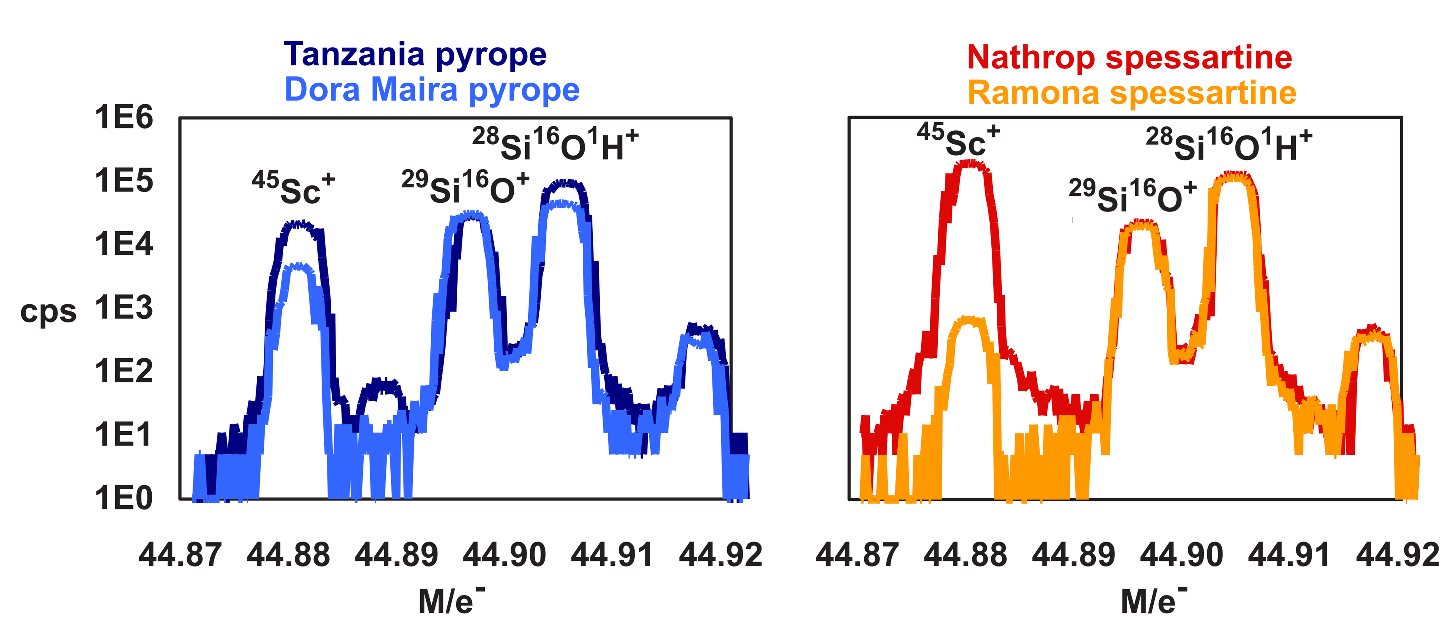

Mass/charge (M/e$^-$) region near $^{45}Sc^+$ in garnet showing nearby interferences.